Molecular Biology of the Cell
Vol. 20, 3930–3940, September 1, 2009

ZO-1 Stabilizes the Tight Junction Solute Barrier through Coupling to the Perijunctional Cytoskeleton

Christina M. Van Itallie,*† Alan S. Fanning,†‡ Arlene Bridges,§ and James M. Anderson‡

Departments of *Medicine and ‡Cell and Molecular Physiology, and §School of Pharmacy, University of North Carolina at Chapel Hill, Chapel Hill, NC 27599

Submitted April 20, 2009; Accepted July 6, 2009
Monitoring Editor: Keith Mostov

ZO-1 binds numerous transmembrane and cytoplasmic proteins and is required for assembly of both adherens and tight junctions, but its role in defining barrier properties of an established tight junction is unknown. We depleted ZO-1 in MDCK cells using siRNA methods and observed specific defects in the barrier for large solutes, even though flux through the small claudin pores was unaffected. This permeability increase was accompanied by morphological alterations and reorganization of apical actin and myosin. The permeability defect, and to a lesser extent morphological changes, could be rescued by reexpression of either full-length ZO-1 or an N-terminal construct containing the PDZ, SH3, and GUK domains. ZO-2 knockdown did not replicate either the permeability or morphological phenotypes seen in the ZO-1 knockdown, suggesting that ZO-1 and -2 are not functionally redundant for these functions. Wild-type and knockdown MDCK cells had differing physiological and morphological responses to pharmacologic interventions targeting myosin activity. Use of the ROCK inhibitor Y27632 or myosin inhibitor blebbistatin increased TER in wild-type cells, whereas ZO-1 knockdown monolayers were either unaffected or changed in the opposite direction; paracellular flux and myosin localization were also differentially affected. These studies are the first direct evidence that ZO-1 limits solute permeability in established tight junctions, perhaps by forming a stabilizing link between the barrier and perijunctional actomyosin.

INTRODUCTION

Tight junctions form size- and charge-selective barriers to the paracellular movement of solutes and ions across epithelia (Powell, 1981; Madara, 1998). More than 40 different cytoplasmic and transmembrane proteins are located at the junction (Gonzalez-Mariscal *et al.*, 2003; Schneeberger and Lynch, 2004; Guillemot *et al.*, 2008) yet there is limited knowledge of how most contribute to the junction's selective sealing properties. The cytoplasmic protein ZO-1 was the first tight junction protein to be identified (Stevenson *et al.*, 1986). It is a member of the MAGUK family of membrane-associated scaffolding proteins (Funke *et al.*, 2005) and contains protein-binding domains for all the major transmembrane barrier proteins: claudins (Furuse *et al.*, 1998; Itoh *et al.*, 1999), occludin (Furuse *et al.*, 1994; Fanning *et al.*, 1998), tricellulin (Ikenouchi *et al.*, 2005; Riazuddin *et al.*, 2006), JAM-A (Martin-Padura *et al.*, 1998; Ebnet *et al.*, 2000), and several components of the perijunctional network of actin and myosin (Tsukita *et al.*, 2001; Hartsock and Nelson, 2008; Yamazaki *et al.*, 2008). Although ZO-1 gene deletions are embryonic lethal in mice (Katsuno *et al.*, 2008), the depletion of ZO-1 in cultured epithelial cell models (Umeda *et al.*, 2004; McNeil *et al.*, 2006) results in only a delay in barrier formation. Once tight junctions are formed in the ZO-1–depleted cells, TER and flux for large (40 kDa) solutes are reported to be essentially normal (Umeda *et al.*, 2004). There is no direct evidence to date suggesting that ZO-1 normally limits solute permeation in an intact tight junction, despite a widely held view that ZO-1 is a functionally critical tight junction component.

Permeation of solutes through the intact tight junction can be described by two components. The first is transport through a system of ~4-Å radius charge-selective claudin-based pores, most often quantified by transepithelial electrical resistance (TER; Powell, 1981); this is a nearly instantaneous electrical assessment (typically <0.25-several seconds) of ionic permeation through the tight junction. TER is determined by the pattern of claudins in the epithelium and their different electrostatic permeability characteristics (Van Itallie and Anderson, 2006; Angelow *et al.*, 2008). The second component is a lower capacity pathway for solutes larger than ~4 Å in radius, which shows no selectivity for ionic charge or size (Adson *et al.*, 1994; Knipp *et al.*, 1997). Although the structural and mechanistic basis of this pathway is unknown, one speculation is that it represents dynamic breaks and resealing in the junction's cell–cell contacts (Sasaki *et al.*, 2003; Watson *et al.*, 2005). This pathway must be measured over longer time periods (typically 60–180 min) by flux of tracers that are larger than the pores, often mannitol (4.2 Å radius; Schultz and Solomon, 1961) or much larger fluorescent dextrans. A more continuous assessment of permeability as a function of molecular radius can be made by determining the permeability for a graded series of noncharged polyethylene glycol oligomers (Watson *et al.*, 2001; Van Itallie *et al.*, 2008); this methods allows simulta-

This article was published online ahead of print in *MBC in Press* (http://www.molbiolcell.org/cgi/doi/10.1091/mbc.E09–04–0320) on July 15, 2009.

† These authors contributed equally to this work.

Address correspondence to: Christina M. Van Itallie (vitallie@med.unc.edu).

neous quantification of flux through both the small claudin-based pores and the low-capacity break pathway.

Although measurement of TER and solute flux are often combined to describe a monolayer's "permeability," they represent different structural and functional characteristics of the barrier, as is evidenced by observations that they do not necessarily change in parallel (Balda *et al.*, 1996; McCarthy *et al.*, 2000). The distinction between these two pathways is important. The first is the physiologically relevant pathway for transepithelial salt and water transport; its charge selectivity, electrical resistance, and level of permeability influences overall transepithelial transport (Diamond, 1977; Powell, 1981). The second pathway is enhanced by pathological insults allowing transepithelial movement of larger material such as antigens, proinflammatory bacterial fragments or even bacteria and viruses (Clayburgh *et al.*, 2004; Mankertz and Schulzke, 2007). Thus, elucidation of the molecular basis for this second pathway is critical to our understanding of barrier disruption in pathological situations.

There is considerable evidence that perijunctional actin and the activity of myosin influence the second, suprapore, pathway (Turner *et al.*, 1997; Madara, 1998). For example, flux is enhanced by disruption of F-actin (Bentzel *et al.*, 1980; Shen and Turner, 2005) or by activation of nonmuscle myosin 2 ATPase activity by myosin light-chain kinase (MLCK; Zolotarevsky *et al.*, 2002; Wang *et al.*, 2005; Su *et al.*, 2009) downstream in the RhoA and Rho kinase (ROCK) signaling pathways (Samarin and Nusrat, 2009). Significantly, ZO-1 binds to several myosin-associated proteins, including cingulin (Cordenonsi *et al.*, 1999) and Shroom2 (Etournay *et al.*, 2007), to multiple proteins that regulate actin dynamics (Hartsock and Nelson, 2008) and to F-actin itself (Fanning *et al.*, 2002). Furthermore, ZO-1 is one of the few cytoplasmic proteins known to bind directly to the transmembrane barrier proteins of the tight junction, a short list that also includes the multi-PDZ protein MUPP1 (Hamazaki *et al.*, 2002) and the homologues ZO-2 (Fanning *et al.*, 1998; Itoh *et al.*, 1999) and ZO-3 (Haskins *et al.*, 1998; Itoh *et al.*, 1999). Thus, ZO-1 is an ideal candidate to provide a crucial link between perijunctional actomyosin activity and the transmembrane barrier proteins.

To address the role of ZO-1 in the intact tight junction we generated stable Madin-Darby canine kidney (MDCK) cell lines expressing ZO-1 short hairpin RNAs (shRNAs) and assessed the tight junction barrier with a variety of assays and after cytoskeletal provocations. ZO-1 depletion resulted in an increase in the permeability specifically for solutes larger than ~4 Å and in morphological changes and reorganization of actin. The barrier in knockdown cells also showed responses different from those in wild-type cells to manipulations affecting actin polymerization and myosin activity. We conclude that ZO-1 is a critical link that stabilizes the barrier for larger solutes and couples it to the myosin–actin cytoskeleton.

MATERIALS AND METHODS

Cell Culture, Immunoblots, Immunofluorescence

Tet-off MDCK II cells (Clontech, Mountain View, CA) were cultured under standard conditions in DMEM (4.5 g/l glucose), 10% fetal bovine serum, and pen-strep. To produce ZO-1 and ZO-2 knockdown cell lines, tet-off MDCK II cells were cotransfected with pSVZeo (Invitrogen, Carlsbad, CA) and a mixture of three different ZO-1 or -2 shRNAs (Supplemental Figure S1) cloned into the BglII/HindIII sites of the pSuper vector (Oligoengine, Seattle, WA). All transfections were performed with Amaxa nucleofector technology (Lonza, Cologne, Germany) using the manufacturer's recommended conditions for MDCK II cells. Stable cell lines were selected in 1 mg/ml zeocin (InvivoGen, San Diego, CA). Antibiotic-resistant clonal cell lines were screened by immunoblotting and immunofluorescence; three separate clones were selected from each of two separate transfections. ZO-1 rescue constructs (see Figure 4A) were cloned into pTRE vector (BD Biosciences, San Jose, CA) and cotransfected into knockdown cells with pTK hyg (BD Biosciences) or pBlast49 (InvivoGen). Antibiotic-resistant clonal cell lines were selected with 200 μg/ml hygromycin (Roche, Nutley, NJ) or 10 μg/ml blastocidin (InvivoGen) and screened as above; at least three independent clones inducibly expressing each of the three rescue constructs were used in further analyses.

For all experiments unless otherwise indicated cells were cultured for 7–10 d on Transwell permeable supports (0.4-μm polyester membrane, 12-mm inserts, Corning, Corning, NY). Immunoblotting and immunofluorescence microscopy of the cultured cells were performed as described previously (Colegio *et al.*, 2002; Van Itallie *et al.*, 2003). Unless otherwise noted, all antibodies were from Invitrogen, Carlsbad, CA). The anti-ZO-1 rat monoclonal was a gift from Dr. Bruce Stevenson (Scripps, La Jolla, CA; Stevenson *et al.*, 1986); the guinea pig anti-human occludin antibody used in Figure 3E was from Hycult Biotechnology (Uden, Netherlands); the myosin 2B (myo2B) antibody was purchased from Covance (Emeryville, CA); the cingulin antibody was a gift from Dr. Sandra Citi (University of Geneva, Switzerland). The anti-human guinea pig polyclonal antibody used in this experiment also recognized the central cilium; this is not seen with other occludin antibodies. Filamentous actin was visualized using rhodamine-phalloidin (Molecular Probes, Invitrogen, Eugene, OR). Affinity-purified Cy-2–, -3–, and -5–labeled secondary antibodies for immunofluorescence were from Jackson ImmunoResearch (West Grove, PA), and IR680/700 and 800 labeled secondary antibodies for immunoblotting were from Invitrogen and Rockland Immunochemicals (Gilbertsville, PA).

Wide-field images were acquired on a Nikon E800 microscope (Melville, NY) using 60× or 100× Plan Apo lenses and an Orca ER cooled CCD camera controlled with the Metamorph Imaging software package (ver. 6.0; Universal Imaging, West Chester, PA). Filter sets and dye combinations have been previously described (Fanning *et al.*, 2002). Confocal images were acquired on a Zeiss LSM510 Meta using a 63× Plan Apo lens (Thornwood, NY). Confocal Stacks and image projections were generated with Zeiss LSM Image Browser (ver. 3.2). All confocal images are maximum density projections of three image planes representing 1.05-μm final depth. Contrast adjustment and montages were generated using Adobe Photoshop (ver. 7.0; San Jose, CA).

Barrier Assays: Polyethylene Glycol, FITC-Dextran and Mannitol Permeability, Transepithelial Electrical Resistance, and Dilution Potentials

Polyethylene glycol (PEG) profiling to determine the size dependence of permeability has been described recently (Van Itallie *et al.*, 2008); to correct the P_{app} of the size-dependent first phase, the second phase is extended after linear regression and subtracted from the first phase (Van Itallie *et al.*, 2008). Determination of [^{3}H]mannitol flux and dilution potentials were performed as described previously (Van Itallie *et al.*, 2001). Dilution potential experiments were performed on cells plated on removable permeable supports (Snapwell, Corning). Transepithelial electrical resistance was determined using plate electrodes placed on either side of the monolayer attached to an EVOM (WPI, Sarasota, FL). FITC-dextran permeability was measured after preincubation of monolayers in Hanks' buffered salt solution (HBSS) containing $CaCl_2$ and $MgSO_4$; fluorescein-conjugated dextran (FD), 3 or 10 kDa (Molecular Probes, Invitrogen), was added to the apical compartment at a concentration of 1 mg/ml, and samples were removed from the basolateral compartment at the indicated times. Dextran flux was identical in the apical-to-basal and basal-to-apical directions over the time course of the experiment, suggesting negligible contribution from transcytosis. Fluorescent-dextran concentrations were quantified using a Typhoon 8600 and Image Quant software (Amersham Pharmacia Biotech, Piscataway, NJ); experimental values were determined by extrapolation from a standard curve of known fluorescent-dextran concentrations using linear regression (GraphPad Prism, San Diego, CA). Apparent Permeabilities (P_{app}) were defined as $(dQ/dt)/AC_o$ (Van Itallie *et al.*, 2008). Statistical analysis (ANOVA, Dunett's and *t* tests) were performed using GraphPad software.

Pharmacologic Reagents

Cytochalasin D and InSolution Y-27632 were purchased from Calbiochem (EMD Biosciences, San Diego, CA); S-(−)-blebbistatin was purchased from Toronto Research Chemicals (North York, ON, Canada).

RESULTS

ZO-1 Knockdown in MDCK Monolayers Changes Cell Contact Morphology and the Organization of Apical Actin

Previous studies demonstrated the requirement for ZO-1 for normal assembly kinetics of the tight junction (Umeda *et al.*,

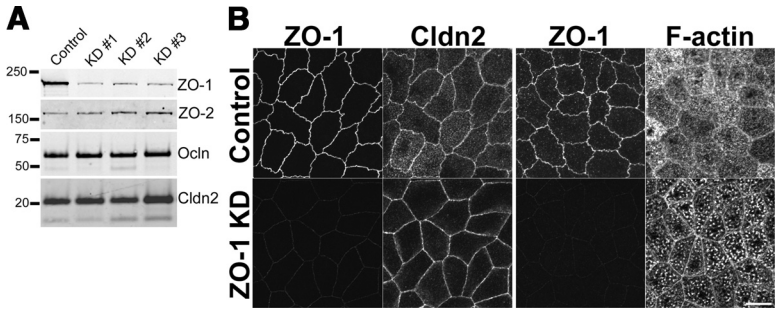

Figure 1. Immunoblot and immunofluorescent characterization of ZO-1 knockdown (KD) MDCK monolayers. (A) Immunoblots of ZO-1 and -2, occludin (ocln), and claudin-2 (cldn2) in control MDCK monolayers and in three independent stable KD clones (1, 2, and 3). KD lines show a 95–97% reduction in ZO-1 levels as quantified by densitometry. KD does not alter the levels of the other proteins. (B) Coimmunolocalization of ZO-1 and claudin-2, and ZO-1 and actin in MDCK control monolayers (top panels) show normally convoluted apical junctional staining. Similar colocalization in KD cells (bottom panels) demonstrates straighter cell junctions and striking redistribution of actin localization. Bar, 10 μm.

2004; McNeil *et al.*, 2006). We used a similar knockdown approach in MDCK cells, but asked whether depletion of ZO-1 had an effect on barrier properties at steady state, i.e., after the junction had sealed. We stably expressed specific shRNAs in the pSuper vector and isolated stable clonal cell lines on the basis of zeocin resistance. Of these, six clones (e.g., see Figure 1A, KD clones 1–3) showed significant reduction of ZO-1 protein levels ranging from 95 to 97% when compared with controls and were chosen for further analysis. The levels of other tight and adherens junction proteins were not consistently affected by knockdown of ZO-1, including ZO-2, occludin, and claudin-2 (Figure 1A). There were also no consistent differences between control and knockdown cells in the expression levels of claudins 1, 3, 4, 7, actin, tricellulin, cadherin, or β-catenin (not shown).

Immunofluorescence microscopic analysis of ZO-1 knockdown cells revealed a striking alteration in cell contact morphology compared with controls. Confluent MDCK II cells typically have convoluted cell–cell contacts at the apical junctional region, as revealed by localization of any of the tight junction proteins, such as ZO-1 or claudin-2 (Figure 1B). Actin is distributed uniformly throughout the cell cortex of MDCK cells and notably is concentrated in basal stress fibers (not shown). In addition, a thin band of cortical actin staining colocalizes with ZO-1 and other cell junction proteins at the apical junctional complex (Figure 1B). When ZO-1 levels are reduced, there is a conversion from tortuous into linear contacts as revealed by the immunolocalization of claudin-2 and the residual ZO-1 (Figure 1B). More dramatically, actin staining is now enriched at both the apical junctional complex and in intense apical dots (Figure 1B). All knockdown cell lines showed this altered junctional morphology and actin reorganization. A conversion from convoluted to straight cell contacts was previously reported after overexpression of Shroom2, a ZO-1–binding protein that also binds actin and myosin VIIIa (Hildebrand, 2005).

Depletion of ZO-1 Destabilizes the Barrier for Large Solutes But Does Not Disrupt the Claudin-based Pores

Solute permeation through the tight junction can be described by two pathways; solutes and ions smaller than ~4 Å radius pass through claudin-based pores; although the physical pathway for larger solutes is unclear, it may represent transient breaks in the barrier (Sasaki *et al.*, 2003; Watson *et al.*, 2005). To determine the role of ZO-1 in regulating these two components of paracellular permeability, we profiled the apparent permeability (P_{app}) of a graded series of PEG oligomers in control and ZO-1 knockdown monolayers. This method allows us to determine simultaneous changes in P_{app} at different molecular radii (Van Itallie *et al.*, 2008). Comparison of MDCK parental cell lines to four separate knockdown clones demonstrated no difference in P_{app} for PEG oligomers below ~4 Å but about a twofold increase in P_{app} for PEG oligomers larger than ~4 Å (Figure 2A). This twofold increase in P_{app} was confirmed by two other flux markers (Figure 2B); [^{3}H]mannitol, which has

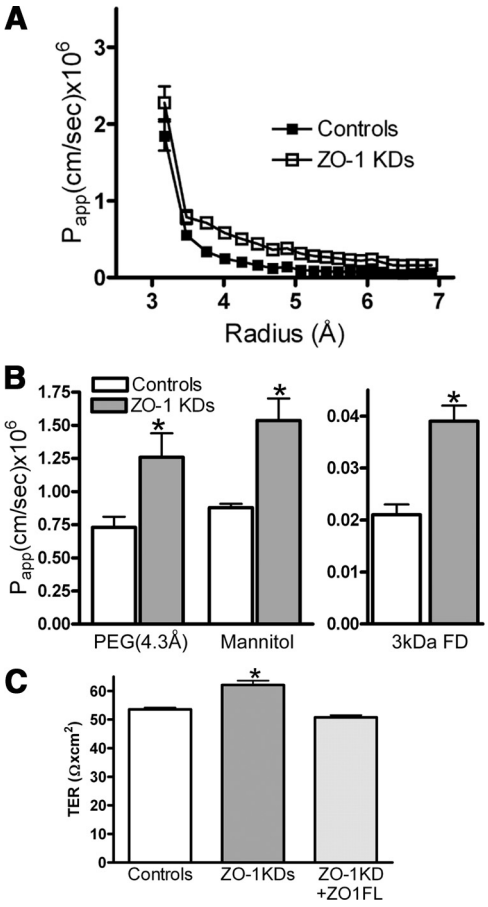

Figure 2. ZO-1 KD cell lines show increased permeability for solutes larger than 3.7Å. (A) P_{app} as a function of PEG radius in MDCK II cells reveals no significant change in flux for small PEGs (3.2- and 3.5-Å radius) but a significant increase in flux for all PEGs 3.7–7.0 Å ($n = 4$ independent KD cell lines, measured on triplicate filters, $p < 0.01$). (B) Significant ($p < 0.01$) increase in flux for larger PEGs was verified by comparison with other methods. P_{app} for PEG with 4.3-Å radius was identical to flux determined using [^{3}H]mannitol (4.2-Å hydrated radius; Schultz and Solomon, 1961), whereas there was a similar increase in P_{app} using 3-kDa FD, both measured using three independent clones, on triplicate filters. (C) In spite of increased flux there was a slight but significant increase in TER in KD cell lines ($n = 6$, three filters each); expression of full-length human ZO-1 (FLZO1) in KD cell line (measure in triplicate) resulted in TER indistinguishable from control.

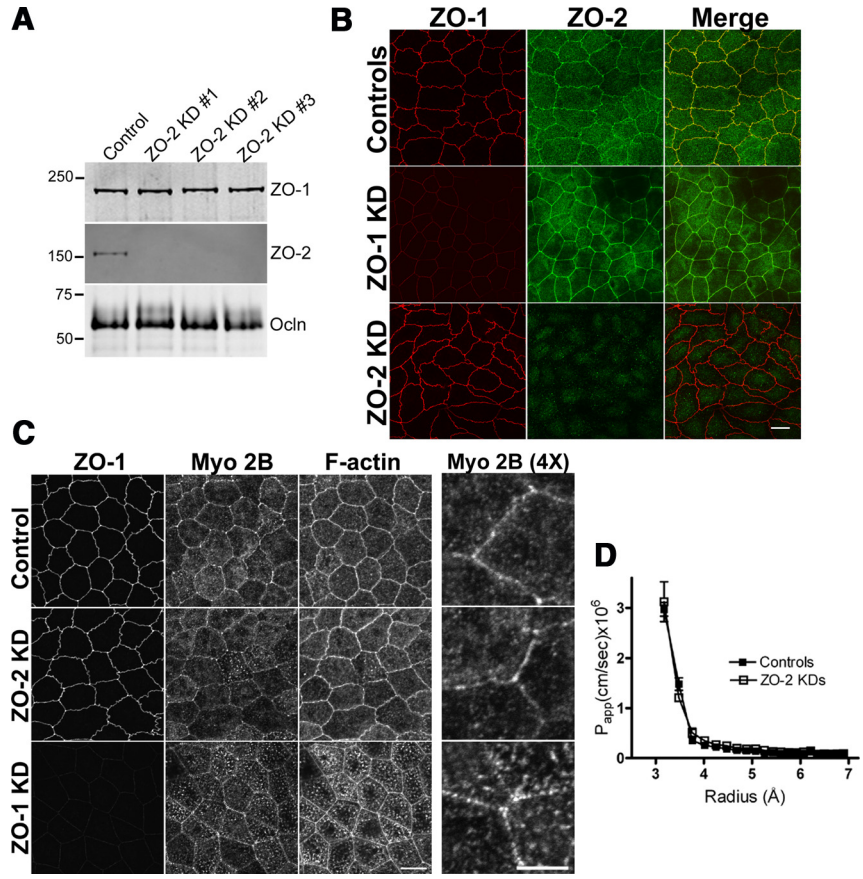

Figure 3. Stable ZO-2 KD in MDCK II cells changes neither cell morphology nor solute permeability. (A) Immunoblot analysis of MDCK control cells and three independent stable ZO-2 KD demonstrate a large decrease in ZO-2 levels (>97%). ZO-2 KD has no effect on ZO-1 or occludin levels. (B) Unlike ZO-1 KDs, ZO-2 KD cells exhibit similar convoluted apical junctions as seen in MDCK control cells. (C) immunofluorescence localization for myosin 2B (myo2B) and actin are similar in MDCK and ZO-2 KD cells, but altered in ZO-1 KD cell lines (see rightmost panel, 4× enlargement of myo2B staining). (D) ZO-2 KD has no effect on P_{app} for any PEG sizes (three independent clones, measured on triplicate filters), nor does it alter TER measurements (not shown).

a hydrated radius of 4.2 Å (Schultz and Solomon, 1961) similar to the hydrated radius of PEG8 (4.3 Å) and 3-kDa FD, which has a molecular radius of ~14Å (Kondoh *et al.*, 2005). Both tracers show the same twofold increase in permeability in the ZO-1 knockdown cells when compared with controls, even though the absolute value of P_{app} for the FD is only 3% that of mannitol. This lower baseline flux of the 3-kDa FD is likely a function of its lower diffusion coefficient. The increased flux of larger compounds in ZO-1 knockdowns is unlikely to represent the formation of a new size-restrictive pore, because there is no evidence for a second inflection point in the permeability data. Instead there is a proportional increase in the flux of all solutes that are larger than the claudin pores, at least for molecules up to 14 Å in radius. When flux of a much larger 10-kDa FD was measured, there was a small but not statistically significant increase in flux in knockdown cells compared with control cells (not shown).

The lack of effect on the flux of molecules through the claudin-based pores suggests that depletion of ZO-1 does not change the biochemical components of this barrier; this is consistent with the lack of effect on the levels and subcellular localization of the tight junction barrier proteins. It is further supported by the finding that ZO-1 knockdown results in a slight but significant increase in TER (Figure 2C), which is the opposite of what would be expected if pores were disrupted. The additional finding that there is no change in the paracellular dilution potential (not shown) is also consistent with the lack of change in the profile of claudins lining the pores in the knockdown cells. The apparent increase in P_{app} in ZO-1–depleted cells for PEGs, which are <4 Å, Figure 2A, does not represent a real increase in permeability of the pores. The smallest PEGs can also pass through the leakier large pathway, so that subtraction of the contribution of the leak pathway from the values for the small-pore pathway reveals that the P_{app} for the smallest PEGs is identical between wild-type and knockdown cells.

ZO-2 Depletion Does Not Replicate the Morphological and Barrier Phenotypes of ZO-1 Depletion

ZO-2 binds to ZO-1, colocalizes at the junction, and shares several key protein-binding domains (Roh and Margolis, 2003; Utepbergenov *et al.*, 2006), suggesting it, like ZO-1, might also regulate solute flux. To test this hypothesis, we used shRNA methods to generate stable clonal MDCK cells lines depleted of ZO-2 (Figure 3). Similar to what was reported in Eph4 cell ZO-2 knockdown cells (Umeda *et al.*, 2006), in MDCK II cells stable ZO-2 depletion did not alter the levels of ZO-1 or occludin (Figure 3A). Immunofluorescent analysis of ZO-2 knockdowns revealed that, unlike ZO-1 knockdowns, ZO-2–depleted cells still showed the convoluted cell–cell contact morphology characteristic of wild-type MDCK II cells (Figure 3B). Also unlike ZO-1 knockdowns, localization of apical myo2B and actin was comparable to that seen in wild-type MDCK cells (Figure 3C). The enlargement in the rightmost panel (Figure 3C, right) reveals that apical myo2B staining appears mostly continuous in both the wild-type and ZO-2 knockdown MDCK cells, but is more punctuate in the ZO-1 knockdowns. Analysis of paracellular solute permeability using PEG size profiling revealed no difference in the P_{app} for any PEG size either below or above the size of claudin pores (Figure 3D); in addition, ZO-2 knockdown did not affect TER (not shown). Thus, unlike ZO-1 the knockdown of ZO-2 had

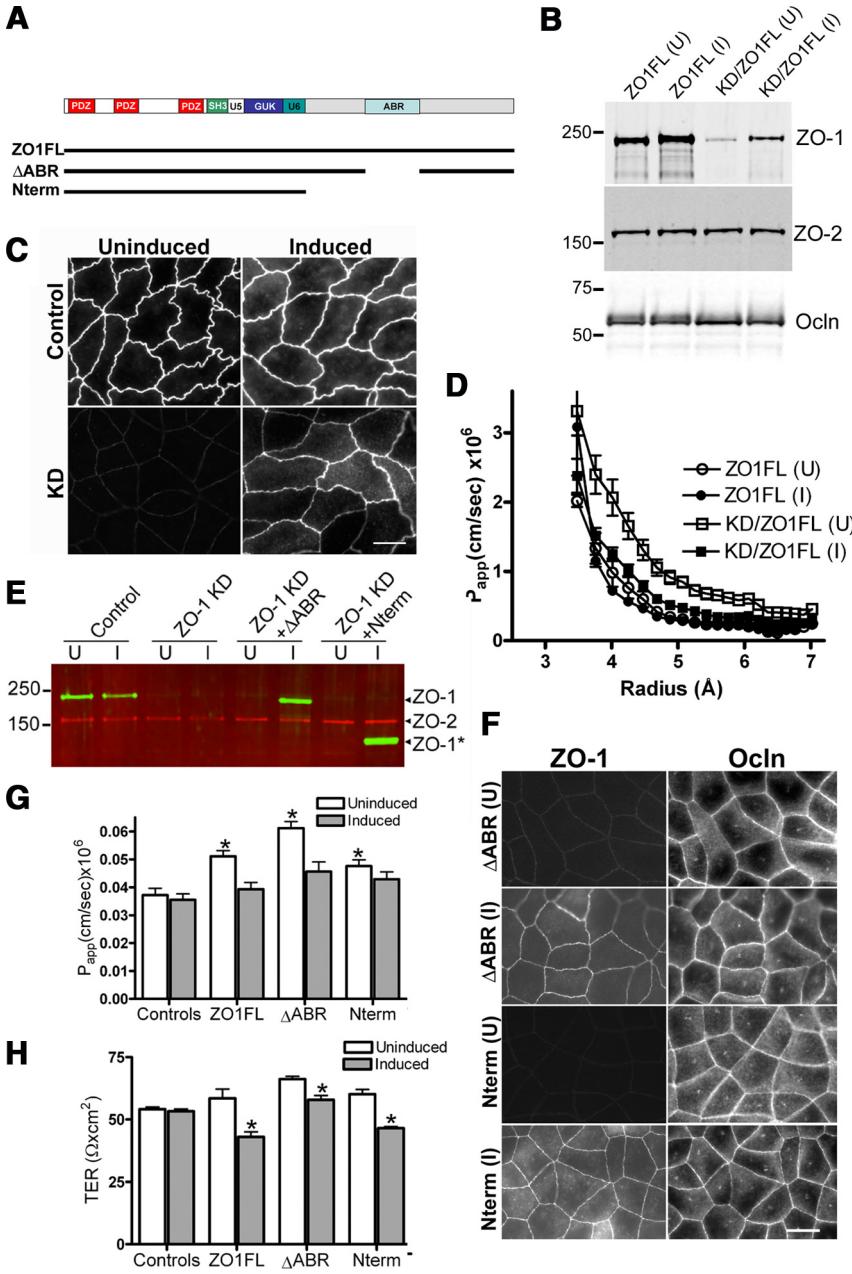

Figure 4. Reexpression of full-length human ZO-1 and -1 fragments restores P_{app} to control levels. (A) Diagram of rescue constructs. Top, ZO1FL full-length human ZO-1; ΔABR deletes only the direct actin-binding region (ΔAA1183-1663; Fanning *et al.*, 2002), Nterm contains amino acids 1-888. The ZO-1 KD cells were created in the MDCK Tet-off cell line, and all rescue constructs were inducible by removal of doxycycline. (B) Expression of FLZO1 in MDCK tet-off cells results in increased ZO-1 levels (135% of control); ZO-1 KD reduces endogenous ZO-1 to 3–5% of control levels. Induction of ZO1FL in KD cells increases ZO-1 levels 3–4-fold over KD values, but only to 15% of control levels. No treatment altered ZO-2 or occludin (ocln) protein levels. (C) Immunofluorescence localization of ZO-1 in control (uninduced, top left panel), MDCK II cells overexpressing human ZO-1 (induced, top right), KD cells (uninduced, bottom left and KD cells induced (bottom right) to express human ZO-1. All constructs show similar tight junction localization. (D) PEG profiling of KD and rescue cell lines. MDCK cells induced (I) or not (U) to express exogenous ZO-1 and KD cells induced (I) to express human ZO-1 all show indistinguishable flux profiles. Only KD cells not induced to express the full-length rescue construct have consistently higher permeability ($p < 0.05$ compared with controls, triplicate filters for each clone per experiment, three separate experiments). (E) ZO-1 rescue fragments (green) are inducible and do not alter ZO-2 levels (red). Endogenous ZO-1 expression levels are not affected by doxycycline induction in either MDCK II or KD cells. When KD cells were stably transfected with rescue constructs as above, transgene expression was not detectable in the uninduced cells (U) but was clearly induced by doxycycline removal (I). ZO-2 levels were not affected by transgene induction. (F) Immunofluorescence localization of induced transgenes demonstrates localization to apical junctional complex and colocalization with occludin. The anti-human guinea pig polyclonal antibody used in this experiment also recognized the central cilium; this is not seen with other occludin antibodies. (G) P_{app} of 3-kDa FD reveals significantly increased flux ($p < 0.05$) in all KD cells lines in the absence of expression of recue constructs; induction of all rescue constructs (one FLZO1 clone measured ± dox, three independent clones for ΔABR and Nterm measured ± dox on triplicate filters) returns P_{app} for FD to levels indistinguishable from control values. (H) Induction of all rescue constructs significantly decreases TER values in all KD cell lines (as above, $p < 0.001$).

no effects on morphology or barrier physiology. The apparent cell size difference in Figure 3B between ZO-1 knockdown cells and controls or ZO-2 knockdowns was not a consistent finding.

ZO-1 or the N-Terminal Half of ZO-1 Rescues the Barrier Defects of ZO-1 Depletion

To determine if reexpression of full-length ZO-1 can rescue the barrier defect caused by depletion of ZO-1, we introduced the ZO-1 knockdown vectors into an MDCK cell line that had been previously engineered to express an inducible human ZO-1 (Fanning *et al.*, 2007). Knockdown vectors were designed to interfere with expression of canine but not human ZO-1. The levels of endogenous canine ZO-1 in these rescue cell lines was significantly reduced (to <5% of that seen in the parental line), comparable to that seen in the knockdown lines described above. Induction of the recombinant full-length human ZO-1 (FLZO1, diagrammed in Figure 4A) in ZO-1 knockdown cell lines restored ZO-1 to levels that were ~12–17% of those seen in the parental lines. Thus, although expression was lower than in wild-type MDCK cells, levels are induced at least threefold over the protein levels in knockdown cells (Figure 4B). Immunofluorescent analysis in ZO-1 knockdown and rescue cells demonstrated that FLZO1 is appropriately localized to tight junctions in induced cells (Figure 4C) in either the presence or absence of the endogenous canine ZO-1 (Figure 4C), although there is a small increase in cytosolic ZO-1 staining when the transgene

is induced in ZO-1 knockdown cells. Notably, there is some increase in tortuosity of the junction contacts when FLZO1 is restored in knockdown cells.

Despite low expression levels, FLZO1 clearly rescues the enhanced permeability seen in ZO1 knockdown cells as revealed by PEG permeability profiling (Figure 4D). Similar to experiments described above, in the absence of FLZO1 expression (□, Figure 4D) the ZO1 knockdown lines demonstrated increased flux of PEG oligomers of 4 Å and above, whereas induction of FLZO1 in these cells restored P_{app} for the larger PEGs to control levels (■, Figure 4D). There was no significant difference in permeability for the PEG oligomers <4 Å in any of the knockdown or rescue cell lines. As expected, expression of FL ZO1 in the parental cell line (which already expresses endogenous ZO-1) had no discernable effect on P_{app} for the small or large PEG oligomers.

To determine critical regions of ZO-1 responsible for rescuing the barrier defect seen in knockdown cells, we transfected ZO-1 knockdown cells with tet-inducible human ZO-1 constructs missing either the actin-binding region (ΔABR, Figure 4A) or encoding only the N-terminal 888 amino acids (Nterm, Figure 4A). Immunoblot analysis demonstrates that both ΔABR and Nterm are efficiently induced and expressed at levels comparable to FLZO1, and neither endogenous ZO-1 nor knockdown ZO-1 levels are affected by the presence (U, uninduced) or absence (I, induced) of doxycycline (the suppressing agent). Furthermore, ZO-2 levels are unchanged by doxycycline treatment (Figure 4E). Immunofluorescent analysis of induced and uninduced cells demonstrates that both deletion constructs localize to the apical junctional complex (Figure 4F). Expression of the ΔABR causes some slight return of the convoluted tight junction morphology seen in control cells, but without a reliable method for quantification, the degree of this rescue is difficult to assess. There is no apparent rescue of the convoluted tight junction morphology with expression of the Nterm construct.

Permeability of 3-kDa FD was significantly increased in all of the MDCK rescue lines before induction of rescue transgenes (Figure 4G), although the level of increase was variable in different clonal cell lines. Nevertheless, induction of any of the transgenes (FL, ΔABR, or Nterm) completely reverses the P_{app} increase to control levels (Figure 4G). Similarly, all of the knockdown cell lines show increased TER relative to MDCK II controls (Figure 4H); in each case, induction of the rescue construct significantly reduces TER to levels similar to MDCK controls or below. These findings suggest that regions sufficient for physiological stabilization of the barrier lie within the amino terminal half of ZO-1.

ZO-1–depleted Cell Lines Demonstrate Increased Sensitivity to Both Cytochalasin D and Ca^{2+} Removal

ZO-1 has been demonstrated to bind F-actin directly (Fanning *et al.*, 1998) and indirectly (reviewed in Hartsock and Nelson, 2008). The phenotype of MDCK knockdown monolayers is consistent with the possibility that ZO-1 is required to maintain the normal perijunctional actin cytoskeleton and stabilize the barrier. Because disruption of the actin cytoskeleton with cytochalasin D is known to disrupt tight junction barrier function (Bentzel *et al.*, 1980; Stevenson and Begg, 1994; Shen and Turner, 2005), we asked whether ZO-1 knockdowns might demonstrate increased sensitivity to cytochalasin D. After culture for 7–10 d on filters, control MDCK II cells are remarkably resistant to cytochalasin D treatment as measured by TER (Figure 5A). In contrast, cytochalasin D treatment of ZO-1 knockdown cells results in a significant time-dependent drop in TER. These results are consistent

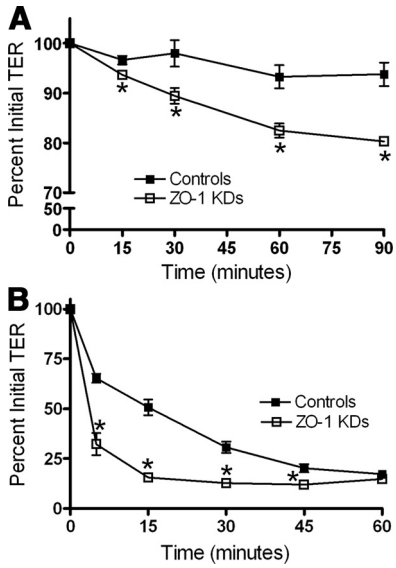

Figure 5. ZO-1 KDs are more sensitive to cytochalasin D treatment and Ca^{2+} removal than are control MDCK cells. (A) MDCK and KD cells cultured for 7 d on Transwell filters were preincubated in HBSS containing Ca^{2+} and Mg^{2+} for 20 min and TER was measured. Monolayers were then changed into fresh media containing either DMSO or 10 μg/ml cytochalasin D in DMSO. TER was measured on triplicate filters at the indicated times; * $p < 0.05$ or less, similar results were obtained with a second KD cell line. (B) MDCK and KD cells were cultured as above; TER was measured and cells were washed four times with Ca^{2+}-free SMEM and then incubated in SMEM supplemented with 10% dialyzed (against EGTA) fetal bovine serum and 5 μM $CaCl_2$. TER was measured at the indicated times, measurements made on triplicate filters; * $p < 0.05$ or less; similar results were obtained with a second KD cell line.

with a role for ZO-1 in stabilizing normal actin organization required to maintain the barrier.

We also tested the role of ZO-1 in stabilizing the barrier after Ca^{2+} removal. Transferring confluent MDCK II cell monolayers into low Ca^{2+} media (5 μM) results in a decrease in TER that reaches a stable level at 60 min (Figure 5B). Ca^{2+} removal from ZO-1 knockdown cells results in a significantly faster decrease in TER, reaching a new plateau level at 15 min. As previously reported by others, we also observed a delay in the reformation of tight junctions after Ca^{2+} replacement in the knockdown cells relative to control cells (not shown). Although it is not known precisely how Ca^{2+} removal leads to barrier loss, our results are again consistent with a role for ZO-1 in tight junction stabilization.

The Barrier Is Functionally Uncoupled from Myosin in ZO-1–depleted Monolayers

Many studies have demonstrated a role for myosin in the regulation of paracellular permeability (reviewed in Turner, 2006; Ivanov, 2008), but the functional links between the tight junction and actomyosin have not been established. To determine whether ZO-1 is such a link, we asked whether depletion of ZO-1 changes the sensitivity of the barrier to agents that alter myosin ATPase activity, namely the ROCK inhibitor Y27632 and myosin inhibitor blebbistatin.

ROCK is thought to activate nonmuscle myosin 2 ATPase through both direct phosphorylation of the regulatory light chain and by inhibition of myosin light chain (MLC) dephosphorylation (Amano *et al.*, 1996; Kimura *et al.*, 1996; Nakai *et al.*, 1997). There is no single model for how myosin controls

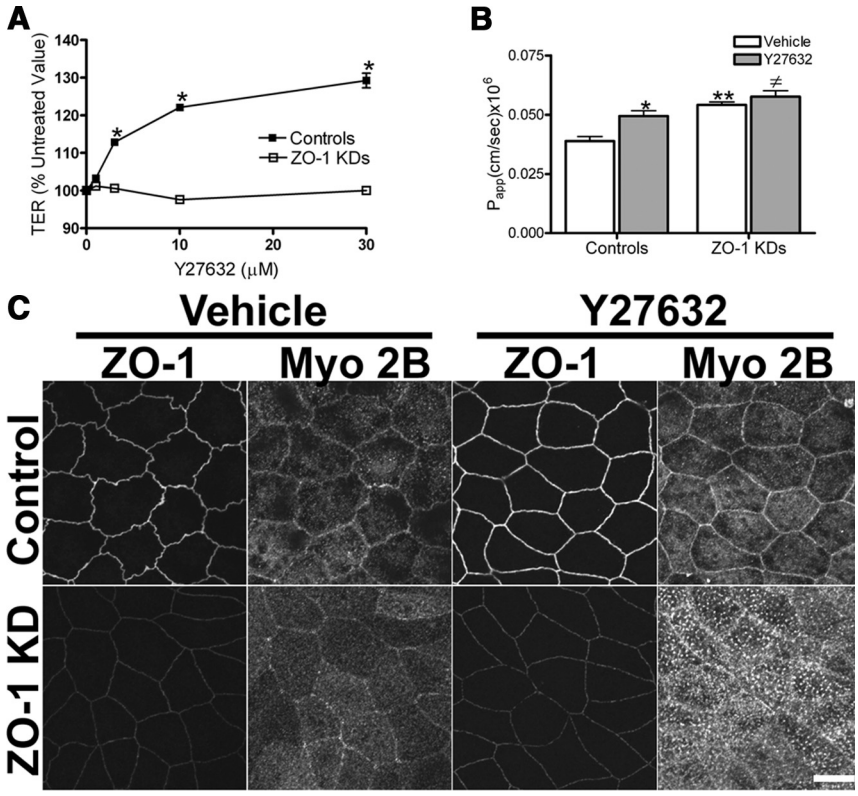

Figure 6. MDCK II control and ZO-1 KD cells show differential sensitivity to the Rho kinase (ROCK) inhibitor Y27632. (A) Cells were cultured on filters for 7 d and then changed into media containing vehicle or the indicated doses of Y27632. TER was measured at 0, 2, 6, and 20 h (shown); there was little difference in effects on TER at any time point. MDCK control but not KD cells demonstrated a dose-dependent (triplicate filters, $p < 0.001$) increase in TER. (B) Cells treated with 30 μM Y27632 for 20 h as above were used for flux measurement; there was a significant increase in P_{app} for 3-kDa FD after treatment with ROCK inhibitor but no further elevation in flux in KDs (triplicate filters, * $p < 0.05$ compared with vehicle, ** $p < 0.001$ compared with vehicle-treated MDCK cells, and # no significant difference with vehicle-treated KD cells.) (C) Immunofluorescence analysis of vehicle and Y27632-treated MDCK and KD cells lines. Ethanol-fixed MDCK monolayers cultured on filters and treated with 30 μM Y27632 for 20 h as above were stained for ZO-1 and Myo2B; Y27632 treatment increased apical junctional immunolocalization of Myo2B in control cells but not in KDs, but increased apical spots in KD cells. Bar, 5 μm.

the barrier. For example, administration of the ROCK inhibitor Y27632 increases basal TER in confluent MDCK cells (Fujita *et al.*, 2000) yet has the opposite effect in T84 cells (Walsh *et al.*, 2001). These differing responses may represent different levels of myosin activation (Ivanov, 2008) or the activity of other downstream targets of ROCK (Riento and Ridley, 2003). With this caveat we tested whether depletion of ZO-1 altered coupling between myosin activity and the barrier. As previously reported, Y27632 increased TER in our wild-type MDCK II cells in a dose-dependent manner (Figure 6A). This increase was similar at 2, 6, and 24 h; the dose dependence at 24 h is shown in Figure 6A. In contrast, ZO-1–depleted monolayers were strikingly insensitive to Y27632 at any dose or time.

Solute permeability showed a similar insensitivity to Y27632. In control MDCK cells 24 h of treatment with Y27632 increased permeability for both 3-kDa FD (Figure 6B) and mannitol (not shown). In contrast, ZO-1 knockdown cells, which have higher basal dextran permeability, failed to show further permeability increases with Y27632 administration. The different sensitivity of these cells to Y27362 correlates with differential response in myosin immunolocalization in control and knockdown cells after Y27632 treatment. myo2B immunofluorescence at apical junctional contacts follows the convoluted cell contacts characteristic of wild-type MDCK cells (Figure 6C), whereas in the ZO-1–depleted cells myo2B follows the straighter cell borders that characterize the knockdowns, with a more punctuate, less continuous distribution (see Figure 3C, 4× magnified images). Treatment of wild-type cells with the ROCK inhibitors decreases the membrane tortuosity of wild-type cells and slightly increases the intensity of myo2B staining at apical cell borders. Administration of the ROCK inhibitor to ZO-1–depleted cells does not increase the intensity of myosin 2B at apical cell contacts, but dramatically increases the amount of myo2B concentrated in scattered apical spots.

Blebbistatin, unlike Y27632, is a direct inhibitor of myosin 2 activity; its administration to confluent MDCK II cell monolayers results in a dose-dependent increase in TER, although this increase is less pronounced than that seen after ROCK inhibition (Figure 7A). However, unlike the effect of the ROCK inhibitor on knockdown cells blebbistatin treatment causes a significant dose-dependent decrease in TER in the ZO-1–depleted cells (Figure 7A). Blebbistatin administration has no effect on permeability in the control cells, whereas in knockdown cells it further elevated 3-kDa FD flux (Figure 7B). In addition, blebbistatin administration resulted in a more pronounced relocalization of myo2B in knockdown cells when compared with control cells (Figure 7C). The reasons for the changes in morphology are unclear, but they are consistent with an influence of ZO-1 on myosin organization, perhaps through its interaction with actin. One important caveat is that only a fraction of the cellular actin and myosin are localized to the tight junction, and the ROCK inhibitor and blebbistatin have multiple cellular actions.

DISCUSSION

In the current study we demonstrate that ZO-1 depletion in MDCK cells results in a size-selective increase in permeability for solutes that are larger than the claudin-based pores. In addition, ZO-1 depletion results in uncoupling of the normal barrier response to inhibition of myosin activity. The barrier defect does not involve a disruption of the small claudin-based pores as measured by the P_{app} of PEGs <4 Å or by TER. In fact, TER, a measure of instantaneous ionic permeability, is slightly but significantly increased in knockdown cells relative to controls. The increased permeability for

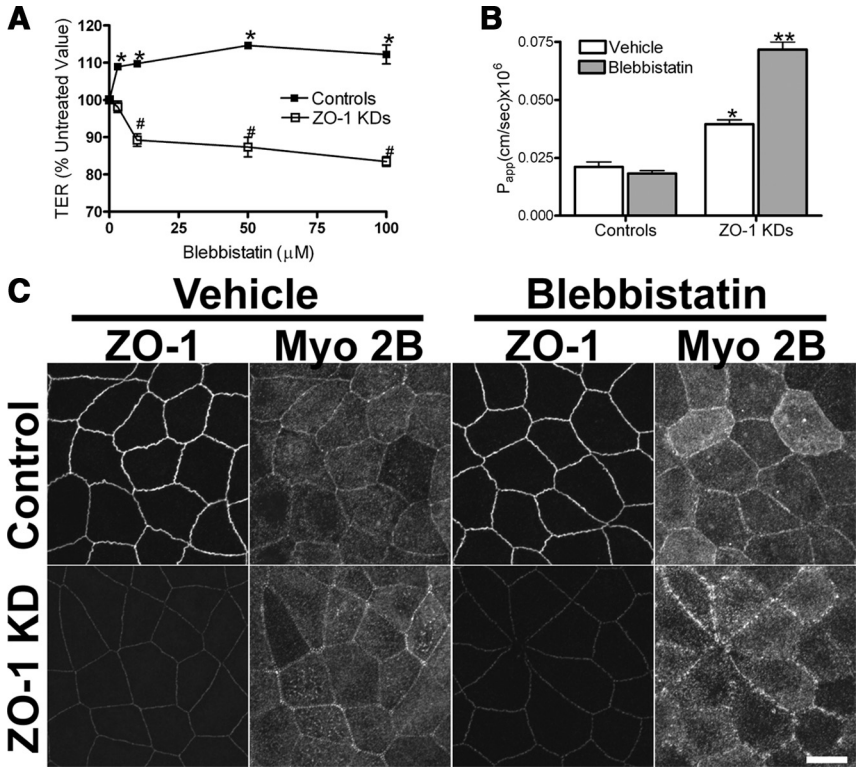

Figure 7. MDCK II control and ZO-1 KD cells show differential sensitivity to the myosin ATPase inhibitor blebbistatin. (A) Cells cultured on filters for 7 d were washed once and preincubated for 20 min in HBSS containing Ca^{2+} and Mg^{2+}. Filters were then changed into fresh HBSS with vehicle or blebbistatin at the indicated doses. TER was measured after 2 h of blebbistatin treatment. MDCK control demonstrated a dose-dependent (* $p < 0.01$) increase in TER; KD cells demonstrate a dose-dependent (# $p < 0.05$) decrease in TER (triplicate filters). (B) Cells treated with 50 μM blebbistatin or vehicle were used for determination of FD flux; there was no change in MDCK control cells with blebbistatin, but blebbistatin treatment resulted in a further significant elevation of P_{app} for 3-kDa FD (* $p < 0.05$ compared with controls, ** $p < 0.001$ compared with vehicle-treated KD cells, triplicate filters). (C) Immunofluorescence analysis of vehicle and blebbistatin-treated MDCK and KD cells lines. Ethanol-fixed MDCK monolayers cultured on filters and treated with vehicle 50 μM blebbistatin for 2 h as above were stained for ZO-1 and myo2B; blebbistatin treatment resulted in greater disorganization of myo2B staining in KD cells than in control cells. Bar, 5 μm.

larger solutes is rescued by expression of both full-length ZO-1 and a truncated construct containing amino-terminal domains that, among other things, binds to all of the know tight junction transmembrane proteins (Figure 8). ZO-1 depletion also results in enhanced sensitivity to Ca^{2+}-depletion and actin disruption with cytochalasin D. Taken together this is the first direct evidence that ZO-1 normally serves to stabilize the barrier and functionally link it to the actin–myosin cytoskeleton.

Although ZO-1 is a universal component of tight junctions and interacts with multiple other tight junction proteins, two recent studies (Umeda *et al.*, 2004; McNeil *et al.*, 2006) reported limited physiological consequences after ZO-1 knockout or knockdown in epithelial cells. In contrast, in the current study we demonstrate a requirement for ZO-1 in normal barrier function in MDCK cells and show that ZO-1–depleted MDCK cells have an altered morphology characterized by a loss of tortuosity at the apical junction contacts and changes in apical actin localization. The reasons for the differences between previously published studies and our findings are likely a function of both cell type and methodology. Umeda *et al.* (2004) used homologous recombination to knockout ZO-1 expression in Eph4 cells and reported no change in flux for 40-kDa FD; we report a consistent increase in flux for a smaller (3 kDa) FD, but like Umeda *et al.* have also found that flux of larger 10-kDa FD was not significantly altered. Modest permeability changes (in our case up to twofold) are more difficult to detect as the tracer size increases, except cases where the barrier is catastrophically opened, for example, by Ca^{2+} depletion. The lack of effect on cell morphology may be related to cell type, because Eph4 cells normally lack the convoluted tight junction staining pattern that characterizes MDCK II cells. Macara and coworkers (McNeil *et al.*, 2006), on the other hand, did not measure flux in their ZO-1 knockdown cell lines; that they did not note a change in morphology is likely to be a function of the fact that they used transient transfection to deplete ZO-1 rather than generating stable cell lines as we have done. A third group (Aijaz *et al.*, 2007) has also generated stable MDCK ZO-1 knockdown cell lines. In contrast to our finding, they did not find an effect on paracellular flux. However, this group reported a decrease in ZO-1 levels only to 25% of control levels, compared with 2–5% remaining in our cell lines. We suspect the residual level of ZO-1 in their cells is the reason for their failure to see change in flux, because this level of ZO-1 expression in our "rescued" cell lines is sufficient to return flux to normal levels.

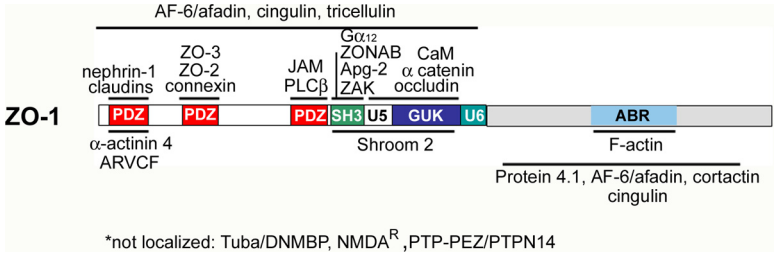

Figure 8. Diagram of reported ZO-1–binding proteins and their binding sites. Original references are cited in Fanning and Anderson (2009). Many ZO-1–binding proteins also bind actin including AF-6, cingulin, ZO-2 and -3, α-catenin, Shroom 2, Protein 4.1, and cortactin. These in turn bind many others that regulate actin dynamics.

In spite of many studies which have reported changes in ZO-1 localization in association with alterations in paracellular permeability (Nusrat *et al.*, 2000; Wang *et al.*, 2005), the finding that ZO-1 depletion results in increased flux in the size-independent pathway is the first demonstration of a clear physiological role for this much studied protein. The observed increase in flux is modest, but it occurs in a background of some residual ZO-1 and minor or no changes in the distribution and levels of most other tight junction proteins. The increased flux is not associated with a decrease in TER or with a change in dilution potential; these outcomes are consistent with the immunolocalization and immunoblot findings that the tight junction transmembrane proteins such as claudins, occludin, and tricellulin are unchanged. Along with the change in flux, the observed alteration in actin localization in the knockdown cells provides clear evidence that ZO-1 is a crucial scaffolding protein, linking a physiologically relevant actin pool to the tight junction barrier. Evidence for a similar role for ZO-2 is lacking, because in our hands, ZO-2 knockdown had no observable physiological effect. This result is different from that reported elsewhere (Hernandez *et al.*, 2007), but could be due to the fact that Hernandez and coworkers tested transiently transfected cells, whereas we analyzed flux in stable knockdowns.

Increased flux for solutes which are larger than the claudin pores in the absence of decreased TER implies that the long-term dynamic characteristics of the barrier are altered by ZO-1 depletion without a compromise in the instantaneous electrical barrier. The tight junction is arranged as a series of continuous claudin-based cell–cell contacts. Multiple barriers presumably provide a fail-safe in case individual contacts transiently break. We speculate that the selective effect of ZO-1 depletion could result from more frequent transient breaks in the contacts but without the simultaneous loss of all of the contacts in series. This would increase permeability for solutes measured over long times but not affect a fast assessment of the barrier with TER. Future studies will test whether ZO-1–depleted junctions are more dynamic.

Previous studies have demonstrated that a ring of filamentous actin normally encircles the apical junctional complex and have indicated that contraction of the ring is associated with changes in cell shape and tight junction permeability (Madara, 1987). Additionally, ultrastructural studies have detected direct contact between actin filaments and the tight junction, although the functional significance of these contacts is unknown (Hirokawa *et al.*, 1983; Madara, 1987). Our studies indicate that F-actin localization is significantly altered in the ZO-1 knockdown cells, with an increase in actin staining at apical junctional complex and into scattered apical dots. These observations suggest that ZO-1 has very specific effects on actin dynamics at the apical junctional complex, perhaps by localizing the activity of cytoskeletal proteins [such as α actinin; Chen *et al.*, 2006), α catenin (Itoh *et al.*, 1997), or shroom2 (Etournay *et al.*, 2007)] or signaling pathways [such as the RhoGEF TUBA (Otani *et al.*, 2006) and $G\alpha_{12}$ (Meyer *et al.*, 2002)] that regulate actin dynamics.

How these changes in actin dynamics or cortical F-actin architecture affect permeability is a matter of speculation. One possibility is that there is a specific cortical actin network that is associated with the barrier and that the assembly or plasticity of this network is organized by ZO-1 (via contacts with cytoskeletal proteins outlined in Figure 8). In the absence of ZO-1, the network does not maintain a normal barrier. It seems unlikely that ZO-1 acts as a direct transducer between the physical force generated by actomyosin activity and components of the barrier. The C-terminus of ZO-1 binds directly to F-actin (outlined in Figure 8); however, because the increased flux is rescued by the Nterm construct, which lacks the direct actin-binding site, direct interactions between ZO-1 and F-actin do not appear essential for barrier stabilization. Instead, our data suggest that indirect contacts via other actin-binding and/or -signaling proteins that bind to the Nterm construct are sufficient.

Whatever the mechanism, our observations suggest that one critical factor is the ability of ZO-1 to link the activity of myosin 2 to the state of the barrier. Perhaps surprisingly, the localization of myosin within the apical junctional complex is only slightly altered in ZO-1 knockdown cells. There is a tendency for it to become less continuous and more punctuate in staining pattern. This pattern, most evident in Figure 7C, is again consistent with loss of normal interactions. Many studies (Nusrat *et al.*, 1995; Jou *et al.*, 1998; Walsh *et al.*, 2001; Benais-Pont *et al.*, 2003; Shen *et al.*, 2006) have implicated myosin activation in changes in paracellular flux downstream of RhoA and MLCK. Despite the subtle changes in myosin 2B localization, there is a clear difference between control and ZO-1 knockdown cells in their responses to pharmacologic inhibition of ROCK or myosin 2 ATPase. This suggests that ZO-1 does not localize myosin 2B, but may still act as a scaffolding protein indirectly regulating myosin activity. For example, ZO-1 knockdown decreases cingulin localization (Umeda *et al.*, 2004; Supplementary Figure S3). Cingulin (and the related protein, paracingulin, Guillemot *et al.*, 2008) have been demonstrated to bind the guanidine nucleotide exchange factor, GEF-H1, which inhibits Rho signaling (Benais-Pont *et al.*, 2003; Aijaz *et al.*, 2005). Decreased tight junction cingulin might increase Rho activation and thus myosin phosphorylation; however, as previously reported, neither cingulin knockout (Guillemot *et al.*, 2004) nor knockdown (Guillemot and Citi, 2006) altered permeability. The role of paracingulin in flux regulation has not yet been tested. Another possibility is that ZO-1 might normally act as a sink for $G\alpha_{12}$, which can bind to the SH3 domain of ZO-1 (Meyer *et al.*, 2002; Sabath *et al.*, 2008; Figure 8) and that ZO-1 depletion would lead to increased activation of Rho A through an increase in accessible $G\alpha_{12}$.

In summary, this is the first direct experimental evidence of a role for ZO-1 in control of paracellular permeability through coupling it to perijunctional actin and myosin. However, providing the evidence that ZO-1 does in fact form a link between the barrier proteins and the cortical cytoskeleton is just a small piece of the puzzle. A cursory inspection of Figure 8 reveals just some of the other proteins that might be important links in this interaction. Unraveling the most relevant of these interactions in the physiological regulation of the tight junction will aid in understanding how barrier integrity is maintained and what components are likely to be involved when the barrier is pathologically compromised.

ACKNOWLEDGMENTS

We thank Dr. M. S. Balda and Karl Matter (University College London), for advice on the development of knockdown cell lines. We thank Jennifer Holmes for technical assistance. Imaging was partially supported by an anonymous grant to the Michael Hooker Microscopy Facility at the University of North Carolina at Chapel Hill. This work was supported by grants from the National Institutes of Health: DK45134 (J.M.A., C.M.V.), DK61397 (J.M.A., A.S.F.), and P30 DK034987.

REFERENCES

Adson, A., Raub, T. J., Burton, P. S., Barsuhn, C. L., Hilgers, A. R., Audus, K. L., and Ho, N. F. (1994). Quantitative approaches to delineate paracellular diffusion in cultured epithelial cell monolayers. J. Pharm. Sci. *83*, 1529–1536.

Aijaz, S., D'Atri, F., Citi, S., Balda, M. S., and Matter, K. (2005). Binding of GEF-H1 to the tight junction-associated adaptor cingulin results in inhibition of Rho signaling and G1/S phase transition. Dev. Cell *8*, 777–786.

Aijaz, S., Sanchez-Heras, E., Balda, M. S., and Matter, K. (2007). Regulation of tight junction assembly and epithelial morphogenesis by the heat shock protein Apg-2. BMC Cell Biol. *8*, 49.

Amano, M., Ito, M., Kimura, K., Fukata, Y., Chihara, K., Nakano, T., Matsuura, Y., and Kaibuchi, K. (1996). Phosphorylation and activation of myosin by Rho-associated kinase (Rho-kinase). J. Biol. Chem. *271*, 20246–20249.

Angelow, S., Ahlstrom, R., and Yu, A. S. (2008). Biology of claudins. Am. J. Physiol. *295*, F867–F876.

Balda, M. S., Whitney, J. A., Flores, C., Gonzalez, S., Cereijido, M., and Matter, K. (1996). Functional dissociation of paracellular permeability and transepithelial electrical resistance and disruption of the apical-basolateral intramembrane diffusion barrier by expression of a mutant tight junction membrane protein. J. Cell Biol. *134*, 1031–1049.

Benais-Pont, G., Punn, A., Flores-Maldonado, C., Eckert, J., Raposo, G., Fleming, T. P., Cereijido, M., Balda, M. S., and Matter, K. (2003). Identification of a tight junction-associated guanine nucleotide exchange factor that activates Rho and regulates paracellular permeability. J. Cell Biol. *160*, 729–740.

Bentzel, C. J., Hainau, B., Ho, S., Hui, S. W., Edelman, A., Anagnostopoulos, T., and Benedetti, E. L. (1980). Cytoplasmic regulation of tight-junction permeability: effect of plant cytokinins. Am. J. Physiol. *239*, C75–CC89.

Chen, V. C., Li, X., Perreault, H., and Nagy, J. I. (2006). Interaction of zonula occludens-1 (ZO-1) with alpha-actinin- *4*, application of functional proteomics for identification of PDZ domain-associated proteins. J. Proteome. Res. *5*, 2123–2134.

Clayburgh, D. R., Shen, L., and Turner, J. R. (2004). A porous defense: the leaky epithelial barrier in intestinal disease. Lab. Invest. *84*, 282–291.

Colegio, O. R., Van Itallie, C. M., McCrea, H. J., Rahner, C., and Anderson, J. M. (2002). Claudins create charge-selective channels in the paracellular pathway between epithelial cells. Am. J. Physiol. *283*, C142–C147.

Cordenonsi, M., D'Atri, F., Hammar, E., Parry, D. A., Kendrick-Jones, J., Shore, D., and Citi, S. (1999). Cingulin contains globular and coiled-coil domains and interacts with ZO-1, ZO-2, ZO-3, and myosin. J. Cell Biol. *147*, 1569–1582.

Diamond, J. M. (1977). Twenty-first Bowditch lecture. The epithelial junction: bridge, gate, and fence. Physiologist *20*, 10–18.

Ebnet, K., Schulz, C. U., Meyer Zu Brickwedde, M. K., Pendl, G. G., and Vestweber, D. (2000). Junctional adhesion molecule interacts with the PDZ domain-containing proteins AF-6 and ZO-1. J. Biol. Chem. *275*, 27979–27988.

Etournay, R., Zwaenepoel, I., Perfettini, I., Legrain, P., Petit, C., and El Amraoui, A. (2007). Shroom2, a myosin-VIIa- and actin-binding protein, directly interacts with ZO-1 at tight junctions. J. Cell Sci. *120*, 2838–2850.

Fanning, A. S., and Anderson, J. M. (2009). Zonula occludens-1 and -2 are cytosolic scaffolds that regulate the assembly of the tight junction. Ann. NY Acad. Sci. *1165*, 113–120.

Fanning, A. S., Jameson, B. J., Jesaitis, L. A., and Anderson, J. M. (1998). The tight junction protein ZO-1 establishes a link between the transmembrane protein occludin and the actin cytoskeleton. J. Biol. Chem. *273*, 29745–29753.

Fanning, A. S., Little, B. P., Rahner, C., Utepbergenov, D., Walther, Z., and Anderson, J. M. (2007). The unique-5 and -6 motifs of ZO-1 regulate tight junction strand localization and scaffolding properties. Mol. Biol. Cell *18*, 721–731.

Fanning, A. S., Ma, T. Y., and Anderson, J. M. (2002). Isolation and functional characterization of the actin binding region in the tight junction protein ZO-1. FASEB J. *16*, 1835–1837.

Fujita, H., Katoh, H., Hasegawa, H., Yasui, H., Aoki, J., Yamaguchi, Y., and Negishi, M. (2000). Molecular decipherment of Rho effector pathways regulating tight-junction permeability. Biochem. J. *346*(Pt 3), 617–622.

Funke, L., Dakoji, S., and Bredt, D. S. (2005). Membrane-associated guanylate kinases regulate adhesion and plasticity at cell junctions. Annu. Rev. Biochem. *74*, 219–245.

Furuse, M., Fujita, K., Hiiragi, T., Fujimoto, K., and Tsukita, S. (1998). Claudin-1 and -2, novel integral membrane proteins localizing at tight junctions with no sequence similarity to occludin. J. Cell Biol. *141*, 1539–1550.

Furuse, M., Itoh, M., Hirase, T., Nagafuchi, A., Yonemura, S., Tsukita, S., and Tsukita, S. (1994). Direct association of occludin with ZO-1 and its possible involvement in the localization of occludin at tight junctions. J. Cell Biol. *127*, 1617–1626.

Gonzalez-Mariscal, L., Betanzos, A., Nava, P., and Jaramillo, B. E. (2003). Tight junction proteins. Prog. Biophys. Mol. Biol. *81*, 1–44.

Guillemot, L., and Citi, S. (2006). Cingulin regulates claudin-2 expression and cell proliferation through the small GTPase RhoA. Mol. Biol. Cell *17*, 3569–3577.

Guillemot, L., Hammar, E., Kaister, C., Ritz, J., Caille, D., Jond, L., Bauer, C., Meda, P., and Citi, S. (2004). Disruption of the cingulin gene does not prevent tight junction formation but alters gene expression. J. Cell Sci. *117*, 5245–5256.

Guillemot, L., Paschoud, S., Pulimeno, P., Foglia, A., and Citi, S. (2008). The cytoplasmic plaque of tight junctions: a scaffolding and signalling center. Biochim. Biophys. Acta *1778*, 601–613.

Hamazaki, Y., Itoh, M., Sasaki, H., Furuse, M., and Tsukita, S. (2002). Multi-PDZ domain protein 1 (MUPP1) is concentrated at tight junctions through its possible interaction with claudin-1 and junctional adhesion molecule. J. Biol. Chem. *277*, 455–461.

Hartsock, A., and Nelson, W. J. (2008). Adherens and tight junctions: structure, function and connections to the actin cytoskeleton. Biochim. Biophys. Acta *1778*, 660–669.

Haskins, J., Gu, L., Wittchen, E. S., Hibbard, J., and Stevenson, B. R. (1998). ZO-3, a novel member of the MAGUK protein family found at the tight junction, interacts with ZO-1 and occludin. J. Cell Biol. *141*, 199–208.

Hernandez, S., Chavez, M. B., and Gonzalez-Mariscal, L. (2007). ZO-2 silencing in epithelial cells perturbs the gate and fence function of tight junctions and leads to an atypical monolayer architecture. Exp. Cell Res. *313*, 1533–1547.

Hildebrand, J. D. (2005). Shroom regulates epithelial cell shape via the apical positioning of an actomyosin network. J. Cell Sci. *118*, 5191–5203.

Hirokawa, N., Keller, T. C., III, Chasan, R., and Mooseker, M. S. (1983). Mechanism of brush border contractility studied by the quick-freeze, deep-etch method. J. Cell Biol. *96*, 1325–1336.

Ikenouchi, J., Furuse, M., Furuse, K., Sasaki, H., Tsukita, S., and Tsukita, S. (2005). Tricellulin constitutes a novel barrier at tricellular contacts of epithelial cells. J. Cell Biol. *171*, 939–945.

Itoh, M., Furuse, M., Morita, K., Kubota, K., Saitou, M., and Tsukita, S. (1999). Direct binding of three tight junction-associated MAGUKs, ZO-1, ZO-2, and ZO-3, with the COOH termini of claudins. J. Cell Biol. *147*, 1351–1363.

Itoh, M., Nagafuchi, A., Moroi, S., and Tsukita, S. (1997). Involvement of ZO-1 in cadherin-based cell adhesion through its direct binding to alpha catenin and actin filaments. J. Cell Biol. *138*, 181–192.

Ivanov, A. I. (2008). Actin motors that drive formation and disassembly of epithelial apical junctions. Front. Biosci. *13*, 6662–6681.

Jou, T. S., Schneeberger, E. E., and Nelson, W. J. (1998). Structural and functional regulation of tight junctions by RhoA and Rac1 small GTPases. J. Cell Biol. *142*, 101–115.

Katsuno, T., *et al.* (2008). Deficiency of zonula occludens-1 causes embryonic lethal phenotype associated with defected yolk sac angiogenesis and apoptosis of embryonic cells. Mol. Biol. Cell *19*, 2465–2475.

Kimura, K., *et al.* (1996). Regulation of myosin phosphatase by Rho and Rho-associated kinase (Rho-kinase). Science *273*, 245–248.

Knipp, G. T., Ho, N. F., Barsuhn, C. L., and Borchardt, R. T. (1997). Paracellular diffusion in Caco-2 cell monolayers: effect of perturbation on the transport of hydrophilic compounds that vary in charge and size. J. Pharm. Sci. *86*, 1105–1110.

Kondoh, M., Masuyama, A., Takahashi, A., Asano, N., Mizuguchi, H., Koizumi, N., Fujii, M., Hayakawa, T., Horiguchi, Y., and Watanbe, Y. (2005). A novel strategy for the enhancement of drug absorption using a claudin modulator. Mol. Pharmacol. *67*, 749–756.

Madara, J. L. (1987). Intestinal absorptive cell tight junctions are linked to cytoskeleton. Am. J. Physiol. *253*, C171–C175.

Madara, J. L. (1998). Regulation of the movement of solutes across tight junctions. Annu. Rev. Physiol. *60*, 143–159.

Mankertz, J., and Schulzke, J. D. (2007). Altered permeability in inflammatory bowel disease: pathophysiology and clinical implications. Curr. Opin. Gastroenterol. *23*, 379–383.

Martin-Padura, I., *et al.* (1998). Junctional adhesion molecule, a novel member of the immunoglobulin superfamily that distributes at intercellular junctions and modulates monocyte transmigration. J. Cell Biol. *142*, 117–127.

McCarthy, K. M., Francis, S. A., McCormack, J. M., Lai, J., Rogers, R. A., Skare, I. B., Lynch, R. D., and Schneeberger, E. E. (2000). Inducible expression of claudin-1-myc but not occludin-VSV-G results in aberrant tight junction strand formation in MDCK cells. J. Cell Sci. *113*, 3387–3398.

McNeil, E., Capaldo, C. T., and Macara, I. G. (2006). Zonula occludens-1 function in the assembly of tight junctions in Madin-Darby canine kidney epithelial cells. Mol. Biol. Cell *17*, 1922–1932.

Meyer, T. N., Schwesinger, C., and Denker, B. M. (2002). Zonula occludens-1 is a scaffolding protein for signaling molecules. Galpha(12) directly binds to the Src homology 3 domain and regulates paracellular permeability in epithelial cells. J. Biol. Chem. *277*, 24855–24858.

Nakai, K., Suzuki, Y., Kihira, H., Wada, H., Fujioka, M., Ito, M., Nakano, T., Kaibuchi, K., Shiku, H., and Nishikawa, M. (1997). Regulation of myosin phosphatase through phosphorylation of the myosin-binding subunit in platelet activation. Blood *90*, 3936–3942.

Nusrat, A., Giry, M., Turner, J. R., Colgan, S. P., Parkos, C. A., Carnes, D., Lemichez, E., Boquet, P., and Madara, J. L. (1995). Rho protein regulates tight junctions and perijunctional actin organization in polarized epithelia. Proc. Natl. Acad. Sci. USA *92*, 10629–10633.

Nusrat, A., Turner, J. R., and Madara, J. L. (2000). Molecular physiology and pathophysiology of tight junctions. IV. Regulation of tight junctions by extracellular stimuli: nutrients, cytokines, and immune cells. Am. J. Physiol. *279*, G851–G857.

Otani, T., Ichii, T., Aono, S., and Takeichi, M. (2006). Cdc42 GEF Tuba regulates the junctional configuration of simple epithelial cells. J. Cell Biol. *175*, 135–146.

Powell, D. W. (1981). Barrier function of epithelia. Am. J. Physiol. *241*, G275–G288.

Riazuddin, S., *et al.* (2006). Tricellulin is a tight-junction protein necessary for hearing. Am. J. Hum. Genet. *79*, 1040–1051.

Riento, K., and Ridley, A. J. (2003). Rocks: multifunctional kinases in cell behaviour. Nat. Rev. Mol. Cell Biol. *4*, 446–456.

Roh, M. H., and Margolis, B. (2003). Composition and function of PDZ protein complexes during cell polarization. Am. J. Physiol. *285*, F377–F387.

Sabath, E., Negoro, H., Beaudry, S., Paniagua, M., Angelow, S., Shah, J., Grammatikakis, N., Yu, A. S., and Denker, B. M. (2008). Galpha12 regulates protein interactions within the MDCK cell tight junction and inhibits tight-junction assembly. J. Cell Sci. *121*, 814–824.

Samarin, S., and Nusrat, A. (2009). Regulation of epithelial apical junctional complex by Rho family GTPases. Front Biosci. *14*, 1129–1142.

Sasaki, H., Matsui, C., Furuse, K., Mimori-Kiyosue, Y., Furuse, M., and Tsukita, S. (2003). Dynamic behavior of paired claudin strands within apposing plasma membranes. Proc. Natl. Acad. Sci. USA *100*, 3971–3976.

Schneeberger, E. E., and Lynch, R. D. (2004). The tight junction: a multifunctional complex. Am. J. Physiol. *286*, C1213–C1228.

Schultz, S. G., and Solomon, A. K. (1961). Determination of the effective hydrodynamic radii of small molecules by viscometry. J. Gen. Physiol. *44*, 1189–1199.

Shen, L., Black, E. D., Witkowski, E. D., Lencer, W. I., Guerriero, V., Schneeberger, E. E., and Turner, J. R. (2006). Myosin light chain phosphorylation regulates barrier function by remodeling tight junction structure. J. Cell Sci. *119*, 2095–2106.

Shen, L., and Turner, J. R. (2005). Actin depolymerization disrupts tight junctions via caveolae-mediated endocytosis. Mol. Biol. Cell *16*, 3919–3936.

Stevenson, B. R., and Begg, D. A. (1994). Concentration-dependent effects of cytochalasin D on tight junctions and actin filaments in MDCK epithelial cells. J. Cell Sci. *107*(Pt 3), 367–375.

Stevenson, B. R., Siliciano, J. D., Mooseker, M. S., and Goodenough, D. A. (1986). Identification of ZO-1, a high molecular weight polypeptide associated with the tight junction (zonula occludens) in a variety of epithelia. J. Cell Biol. *103*, 755–766.

Su, L., Shen, L., Clayburgh, D. R., Nalle, S. C., Sullivan, E. A., Meddings, J. B., Abraham, C., and Turner, J. R. (2009). Targeted epithelial tight junction dysfunction causes immune activation and contributes to development of experimental colitis. Gastroenterology *136*, 551–563.

Tsukita, S., Furuse, M., and Itoh, M. (2001). Multifunctional strands in tight junctions. Nat. Rev. Mol. Cell Biol. *2*, 285–293.

Turner, J. R. (2006). Molecular basis of epithelial barrier regulation: from basic mechanisms to clinical application. Am. J. Pathol. *169*, 1901–1909.

Turner, .R., Rill, B. K., Carlson, S. L., Carnes, D., Kerner, R., Mrsny, R. J., and Madara, J. L. (1997). Physiological regulation of epithelial tight junctions is associated with myosin light-chain phosphorylation. Am. J. Physiol. *273*, C1378–C1385.

Umeda, K., Ikenouchi, J., Katahira-Tayama, S., Furuse, K., Sasaki, H., Nakayama, M., Matsui, T., Tsukita, S., Furuse, M., and Tsukita, S. (2006). ZO-1 and ZO-2 independently determine where claudins are polymerized in tight-junction strand formation. Cell *126*, 741–754.

Umeda, K., Matsui, T., Nakayama, M., Furuse, K., Sasaki, H., Furuse, M., and Tsukita, S. (2004). Establishment and characterization of cultured epithelial cells lacking expression of ZO-1. J. Biol. Chem. *279*, 44785–44794.

Utepbergenov, D. I., Fanning, A. S., and Anderson, J. M. (2006). Dimerization of the scaffolding protein ZO-1 through the second PDZ domain. J. Biol. Chem. *281*, 24671–24677.

Van Itallie, C., Rahner, C., and Anderson, J. M. (2001). Regulated expression of claudin-4 decreases paracellular conductance through a selective decrease in sodium permeability. J. Clin. Invest. *107*, 1319–1327.

Van Itallie, C. M., and Anderson, J. M. (2006). Claudins and epithelial paracellular transport. Annu. Rev. Physiol. *68*, 403–429.

Van Itallie, C. M., Fanning, A. S., and Anderson, J. M. (2003). Reversal of charge selectivity in cation or anion-selective epithelial lines by expression of different claudins. Am. J. Physiol. *285*, F1078–F1084.

Van Itallie, C. M., Holmes, J., Bridges, A., Gookin, J. L., Coccaro, M. R., Proctor, W., Colegio, O. R., and Anderson, J. M. (2008). The density of small tight junction pores varies among cell types and is increased by expression of claudin-2. J. Cell Sci. *121*, 298–305.

Walsh, S. V., Hopkins, A. M., Chen, J., Narumiya, S., Parkos, C. A., and Nusrat, A. (2001). Rho kinase regulates tight junction function and is necessary for tight junction assembly in polarized intestinal epithelia. Gastroenterology *121*, 566–579.

Wang, F., Graham, W. V., Wang, Y., Witkowski, E. D., Schwarz, B. T., and Turner, J. R. (2005). Interferon-gamma and tumor necrosis factor-alpha synergize to induce intestinal epithelial barrier dysfunction by up-regulating myosin light chain kinase expression. Am. J. Pathol. *166*, 409–419.

Watson, C. J., Hoare, C. J., Garrod, D. R., Carlson, G. L., and Warhurst, G. (2005). Interferon-gamma selectively increases epithelial permeability to large molecules by activating different populations of paracellular pores. J. Cell Sci. *118*, 5221–5230.

Watson, C. J., Rowland, M., and Warhurst, G. (2001). Functional modeling of tight junctions in intestinal cell monolayers using polyethylene glycol oligomers. Am. J. Physiol. *281*, C388–C397.

Yamazaki, Y., Umeda, K., Wada, M., Nada, S., Okada, M., Tsukita, S., and Tsukita, S. (2008). ZO-1- and ZO-2-dependent integration of myosin-2 to epithelial zonula adherens. Mol. Biol. Cell *19*, 3801–3811.

Zolotarevsky, Y., Hecht, G., Koutsouris, A., Gonzalez, D. E., Quan, C., Tom, J., Mrsny, R. J., and Turner, J. R. (2002). A membrane-permeant peptide that inhibits MLC kinase restores barrier function in in vitro models of intestinal disease. Gastroenterology *123*, 163–172.